Supplementary materials

Green and robust chitin hydrogel toward high-performance Zn anode for sustainable energy storage

Yuyang Yan[#], Haodong Zhang[#,*], Yanbo Zhu, Xiaotang Gan, and Jinping Zhou[*]

Hubei Engineering Center of Natural Polymers-based Medical Materials, Key Laboratory of Biomedical Polymers of Ministry of Education, College of Chemistry and Molecular Sciences, Wuhan University, Wuhan 430072, China

*Corresponding author

E-mail address: zhoujp325@whu.edu.cn (J. Zhou); zhanghdwhu@whu.edu.cn (H. Zhang)

1. Experimental Section

Chemical and Materials

The raw chitin powder was purchased from Aladdin Biochemical Co. Ltd. (Shanghai, China). To remove the protein and mineral substances, the chitin powder was purified by 5 wt% sodium hydroxide (NaOH) and 5 wt% hydrochloric acid (HCl) solution for 24 h, respectively. NaOH, urea, ethanol, NH_4VO_3, $H_2C_2O_4\cdot 2H_2O$, $ZnSO_4$, polytetrafluoroethylene (PTFE)，isopropyl alcohol and zinc foil (thickness of 100 μm) were purchased from Shanghai Chemical Reagent Co. Ltd. (Shanghai, China). Ketjenblack EC-600JD (KB) carbon was purchased from Kelude New Energy Technology Co., Ltd. (Guangdong, China). Glass fiber Diaphragm (GF/D) was purchased from Whatman Corporation (Maidstone, UK). All reagents were analytical pure and used as received unless otherwise noted.

Preparation of Chitin Solution

The purified chitin powder was dispersed in a NaOH (15 wt%)/urea (4 wt%) aqueous solution to form a 5 wt % suspension. Subsequently, the suspension was frozen in a cryogenic bath at −40 °C for 12 h. After thawing, the purified chitin was completely dissolved to form a clear and viscous solution, and then was defoamed by centrifugation at 6000 rpm for 10 min at 5 ℃.

Preparation of Chitin Hydrogels

The transparent and viscous chitin solution was spread onto a glass plate to form liquid film (about 0.5 mm) by casting method, then immersed into different ethanol volume fractions of ethanol/water solution for 12 h followed by the complete rinsing with water to obtain chitin hydrogel (CTH-gel). The hydrogel was coded as CTHx, where x is the volume fraction of ethanol. The CTZ-gel electrolyte was prepared by soaking the CTH100 hydrogel in 2 M $ZnSO_4$ for 12 h.

Preparation of NVO Cathode

The NVO cathode material was synthesized by a hydrothermal method.[1] Firstly, 1.17 g of NH_4VO_3 and 1.89 g of $H_2C_2O_4 \cdot 2H_2O$ were added into 70 mL of DI water under magnetically stirring. The solution was then transferred to a 100 mL Teflon-lined autoclave and heated at 140 ℃ for 12 h. After cooling to room temperature naturally, the solid was collected and washed repeatedly with DI water, and then vacuum drying at 80 °C for 12 h to finally obtain the NVO powder.

Characterizations

X-ray photoelectron spectroscopy (XPS) spectra were collected by a Thermo Scientific K-Alpha. Fourier transform infrared (FT-IR) spectra were recorded on a Nicolet 5700 spectrometer (Thermo Nicolet, USA) with an attenuated total reflection (ATR) accessory in the wavenumber range from 4000 to 400 cm^{-1}. X-ray diffraction (XRD) measurements were performed on a Miniflex600 diffractometer (Rigaku, Japan). Using CuKα radiation ($\lambda = 0.154$ nm) at 40 kV and 15 mA, the patterns were recorded in the 2θ region from 5° to 80° at a scanning speed of 5° min^{-1}. Field emission scanning electron microscopy (FE-SEM) observations and energy-dispersive X-ray spectroscopy (EDS) were performed on a MERLIN Compact microscopy (Zeiss, Germany). The gelation time of the chitin hydrogels were studied using a Discovery HR-2 rheometer (TA Instruments) at 25 °C. Hydrogel samples were freeze-dried in a freeze-dryer (Christ ALPHA, Germany) before characterization, and the dried specimens (frozen in liquid nitrogen, snapped immediately, and then freeze-dried) were coated with gold vapor. Topographic images of the surfaces of Zn anodes were observed on an atomic force microscopy (AFM, Asylum Research, UK) in dynamic contact mode.

Mechanical Tests

All mechanical tests were performed at 25 ℃ and 50 % relative humidity using a universal tensile-compressive tester (Model 5576, INSTRON, USA) equipped with a 1000 N load cell. For tension, the hydrogel with square shape (length of 30 mm, width of 10 mm, and thickness of 0.3 mm) was measured at a rate of 50 mm min^{-1}. For compression, the hydrogel with cylindrical shape (height of 5 mm and diameter of 5 mm) was measured at a rate of 10 mm min^{-1}. The elastic modulus and toughness could be calculated from the stress-strain curves.

Soil Degradation Tests

The CTZ-gel and glass fiber (GF) separators were cut into discs with a diameter of 16 mm, wrapped in nylon mesh (500 mesh), and buried in loose natural soil below 20 cm. The degraded samples were evaluated over a period of 0-70 days by using digital photographs and recording the mass change to study the degradation kinetics.

Electrochemical Measurements

The NVO cathode was prepared by mixing NVO powder, Ketjenblack EC-600JD (KB) carbon, and polytetrafluoroethylene (PTFE) binder in a mass ratio of 75:15:10, using a mixed solvent of isopropyl alcohol and water. The resulting homogeneous paste was rolled into a thin film, which was then dried at 70 °C in air overnight and punched into disks with a diameter of 8 mm and an active material mass loading of 3.5−4.0 mg cm^{-2}. The disks were pressed onto stainless steel (SS) meshes as current collectors before cell assembly. CR2032-type coin cells were assembled in an air atmosphere for most electrochemical measurements. A GF membrane (GF/D, Whatman, diameter of 16 mm) was used as the separator, with 100 μL of electrolyte solution (2 M $ZnSO_4$). The CTZ-gel was directly used as electrolyte and separator. The Zn||Zn, Zn||Cu, and Zn||NVO coin cells were fabricated by using Zn foils (100 μm thickness, 99.99% purity) and Cu foils (20 μm thickness), all with a diameter of 12 mm, along with the previously mentioned NVO electrodes. All the electrochemical measurements were operated at 25 °C unless otherwise specified. The discharge−charge measurements of the above cells were conducted on a battery testing system (CT-4008T, Neware, China). Cyclic voltammetry (CV), linear scan voltammetry (LSV), chronoamperometry (CA), and electrochemical impedance spectroscopy (EIS) were carried out on an electrochemical workstation (1470E, Solartron analytical, USA).

The ionic conductivities (σ) were obtained from EIS measurements and calculated using the following equation,

$$\sigma = \frac{l}{RA} \tag{1}$$

where l, R, and A are the thickness, bulk resistance, and area of the SS electrode, respectively.

The desolvation process of Zn^{2+} ions are usually the rate-limiting step of Zn deposition, which can be expressed by the activation energy (E_a) in the Arrhenius equation,

$$\frac{1}{R_{ct}} = A\mathrm{e}^{-\left(\frac{E_a}{RT}\right)} \tag{2}$$

where R_{ct} is the charge transfer resistance, A is the frequency factor, R is the gas constant, and T is the absolute temperature.

Calculation Details

All DFT calculations were performed using Gaussian 16 software. The binding energy (E_b) of Zn^{2+} ions with a specified molecule (M) was calculated using the following equation,

$$E_b = E(Zn^{2+}\text{-M}) - E(Zn^{2+}) - E(M) \tag{3}$$

where M is $6H_2O$ or the simplified model molecule of chitin, and $E(Zn^{2+}\text{-M})$, $E(Zn^{2+})$, and E(B) are the Gibbs free energies of Zn^{2+}-M complex, Zn^{2+} ions, and M, respectively.

2. Supplementary Figures

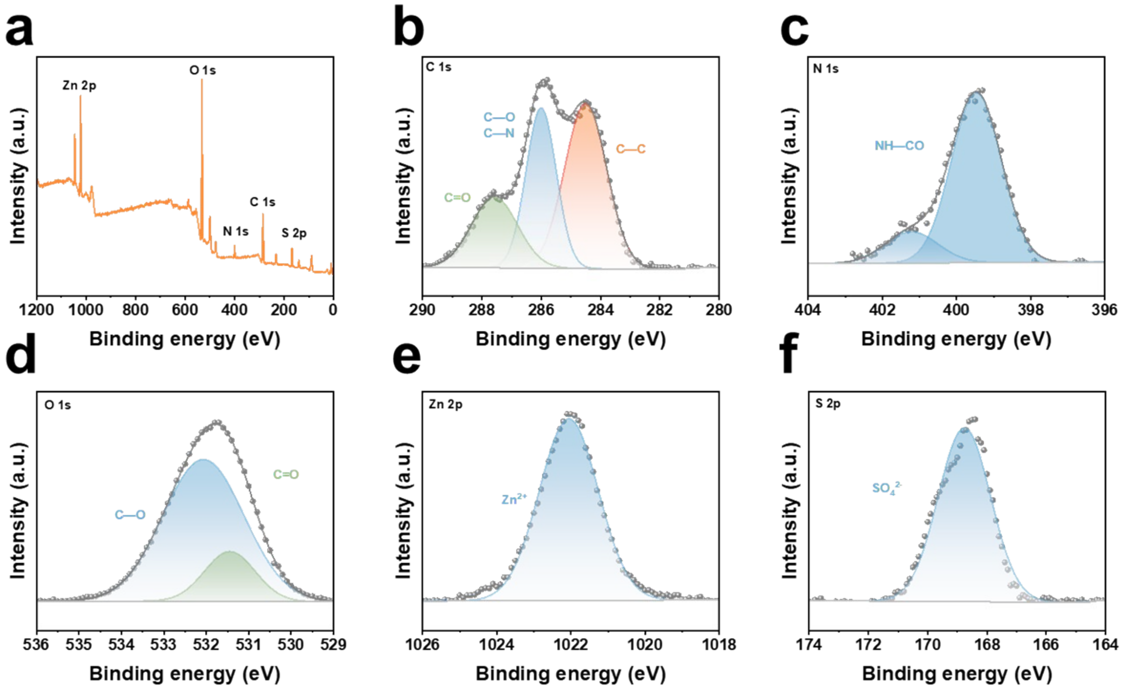

Fig. S1. XPS spectra of the CTZ-gel: (a) full survey; (b) C 1s; (c) N 1s; (d) O 1s; (e) Zn 2p; (f) S 2p spectra.

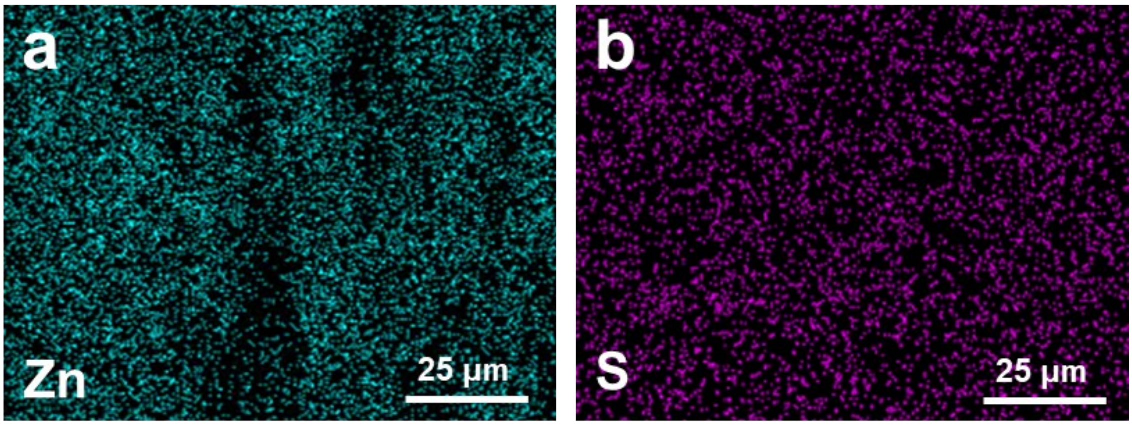

Fig. S2. EDS mapping images of CTZ-gel.

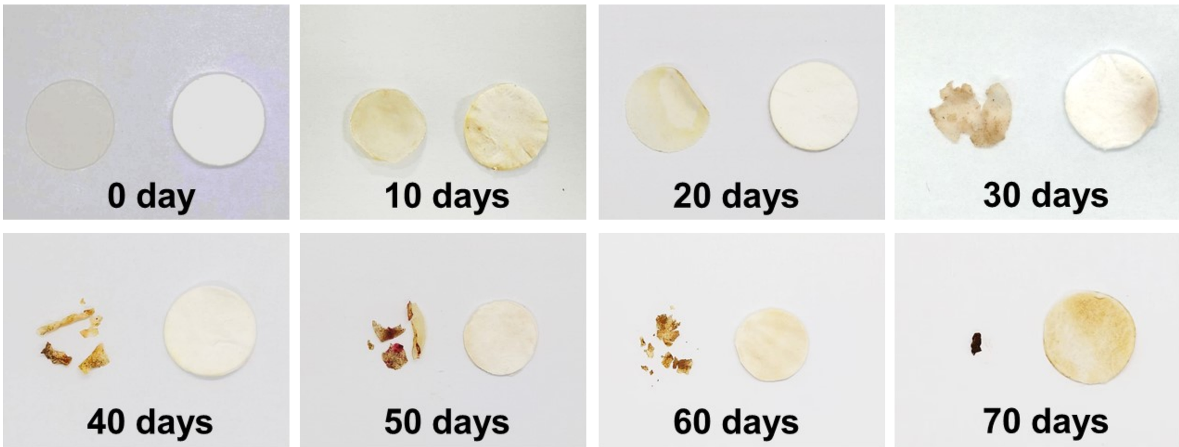

Fig. S3. Photos of degradation behaviors of CTZ-gel and GF on different days.

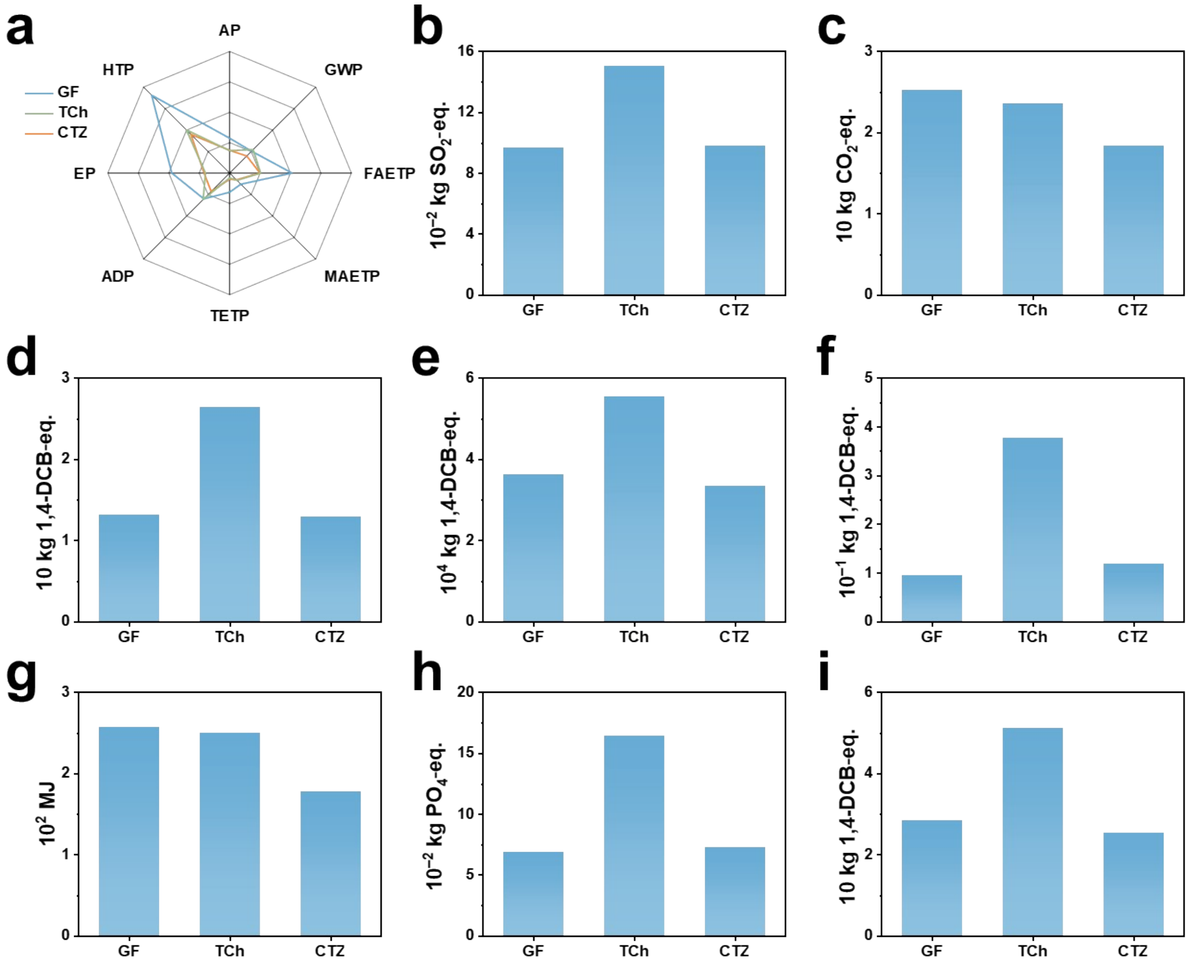

Fig. S4. Environmental impacts of (a) various electrolytes in the categories of: (b) acidification potential (AP), (c) global warming potential (GWP), (d) freshwater and (e) marine ecotoxicity potential (FAETP and MAETP), (f) terrestrial ecotoxicity potential (TETP), (g) abiotic depletion potential (ADP), (h) eutrophication potential (EP), and (i) human toxicity potential (HTP).

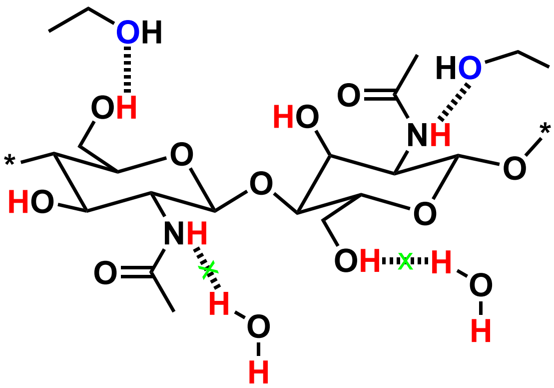

Fig. S5. Illustration for the crosslinking process of chitin molecule in aqueous ethanol solutions.

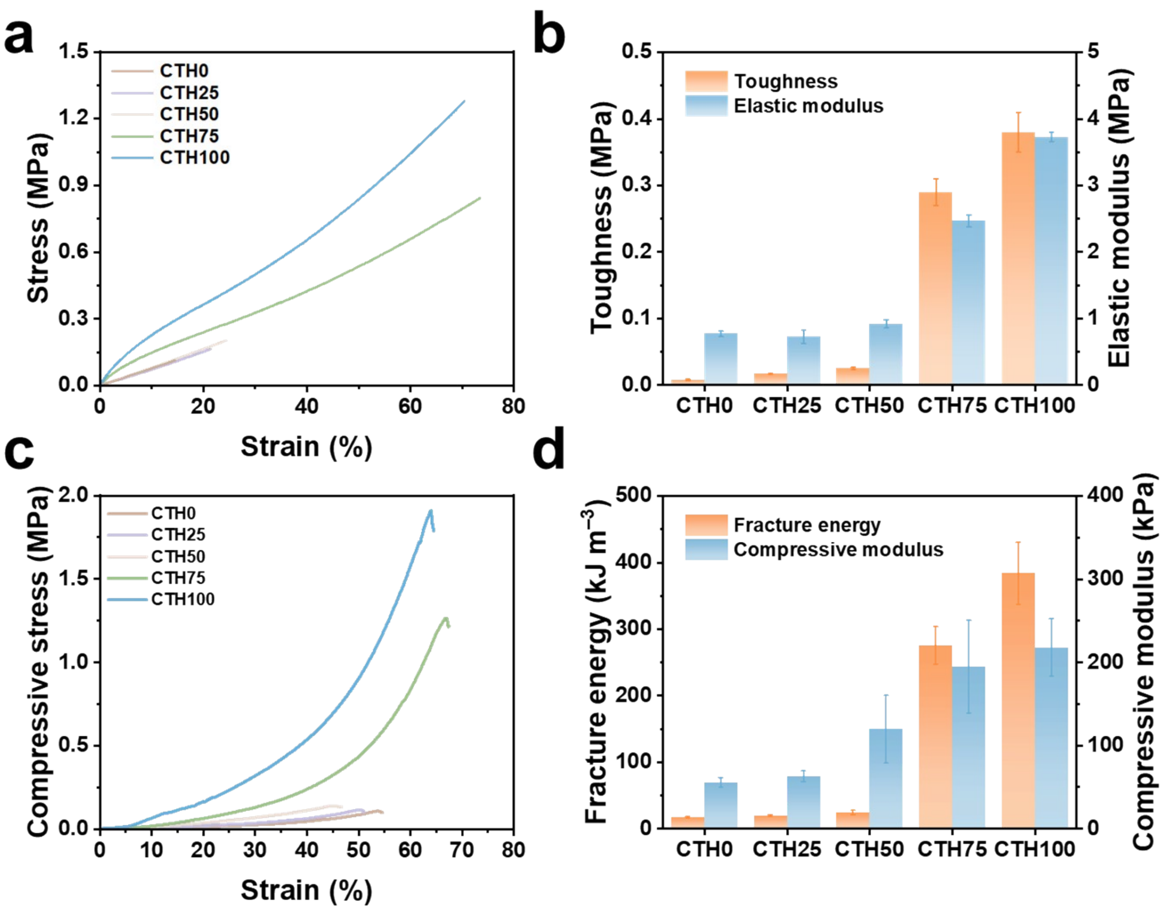

Fig. S6. (a) Tensile stress−strain curves of the chitin hydrogels, and (b) the corresponding toughness and elastic modulus. (c) Compressive stress−strain curves of the chitin hydrogels and (d) the corresponding fracture energy and compressive modulus.

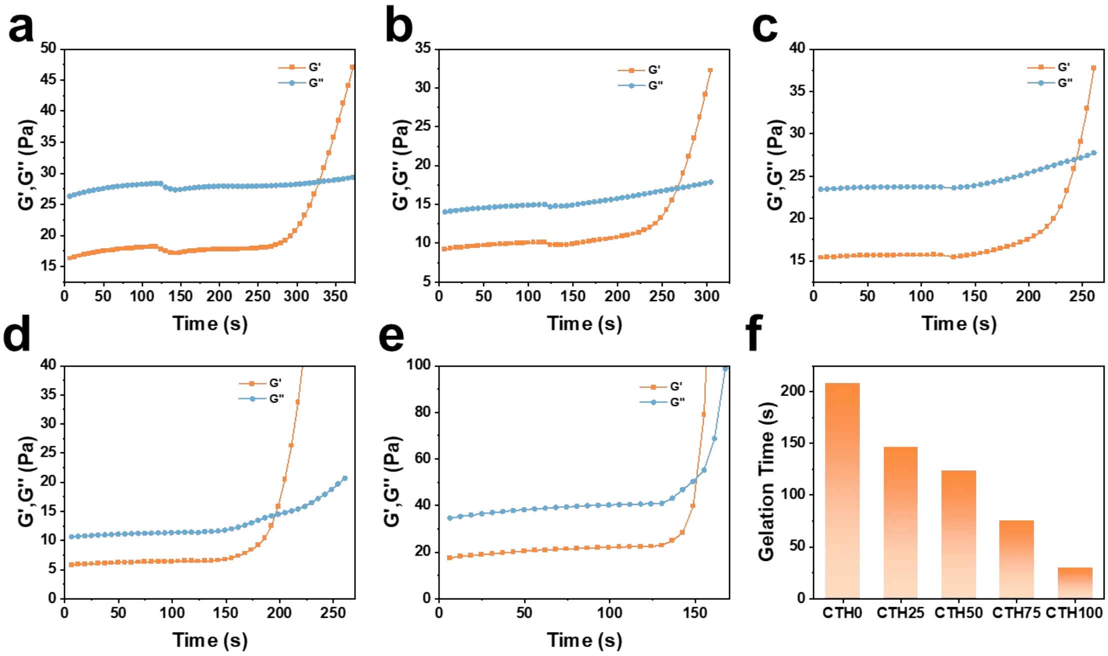

Fig. S7. Time dependence of storage modulus G’ and loss modulus G” for chitin solutions under various concentrations of ethanol: (a) CTH0; (b) CTH25; (c) CTH50; (d) CTH75; (e) CTH100. (f) The gelation time of chitin solution under various concentrations of ethanol.

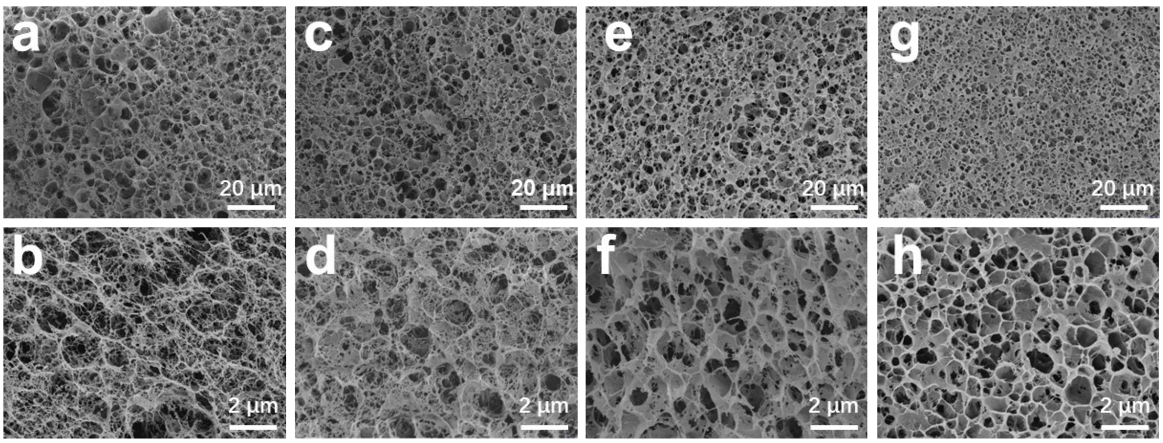

Fig. S8. Cross-sectional FE-SEM image of chitin hydrogels: (a-b) CTH0; (c-d) CTH25; (e-f) CTH50; (g-h) CTH75.

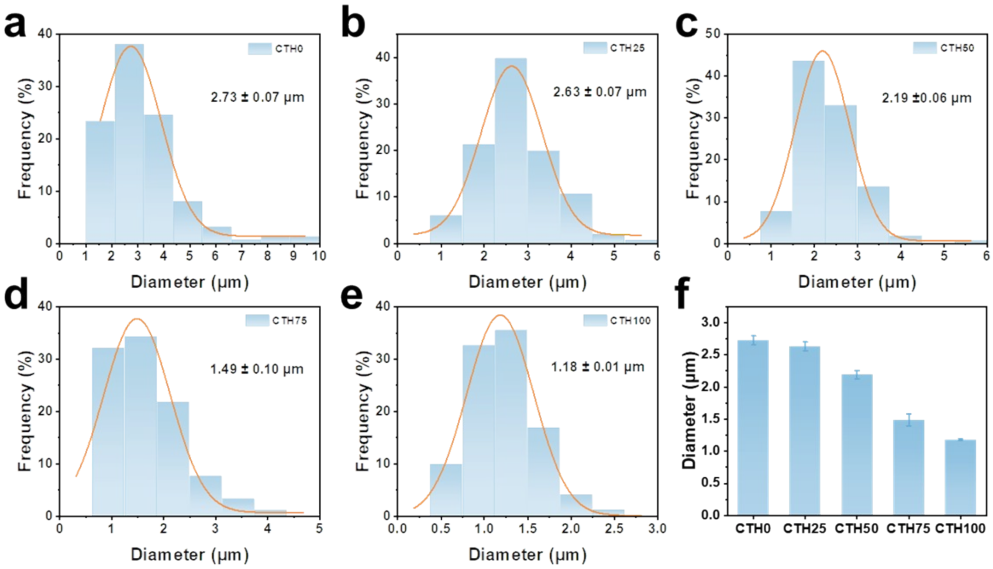

Fig. S9. Frequency distribution statistical chart of different chitin hydrogels obtained from Figure S7: (a) CTH0; (b) CTH25; (c) CTH50; (d) CTH75; (e) CTH100. (f) Statistical chart of aperture of different chitin hydrogels.

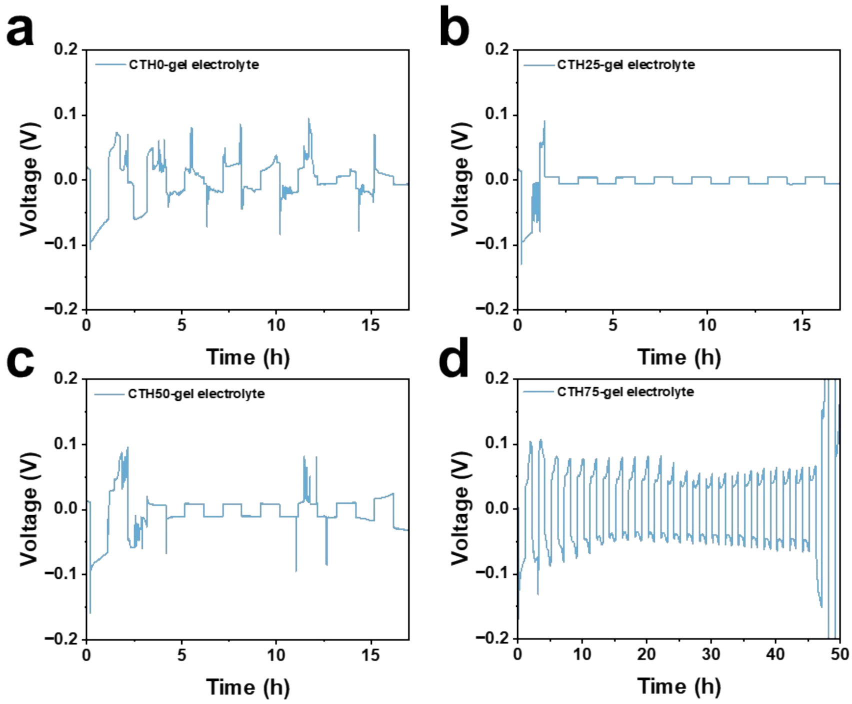

Fig. S10. Voltage−time profile comparison of Zn||Zn cells with current density and capacity of 1 mA cm^{-2}/1 mAh cm^{-2} using the electrolyte of: (a) CTH0, (b) CTH25, (c) CTH50, (d) CTH75.

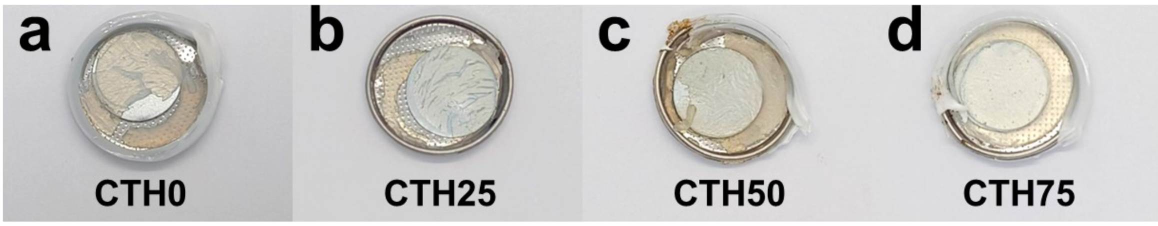

Fig. S11. Photographs of different chitin hydrogel disassembled from the Zn||Zn cells: (a) CTH0; (b) CTH25; (c) CTH50; (d) CTH75.

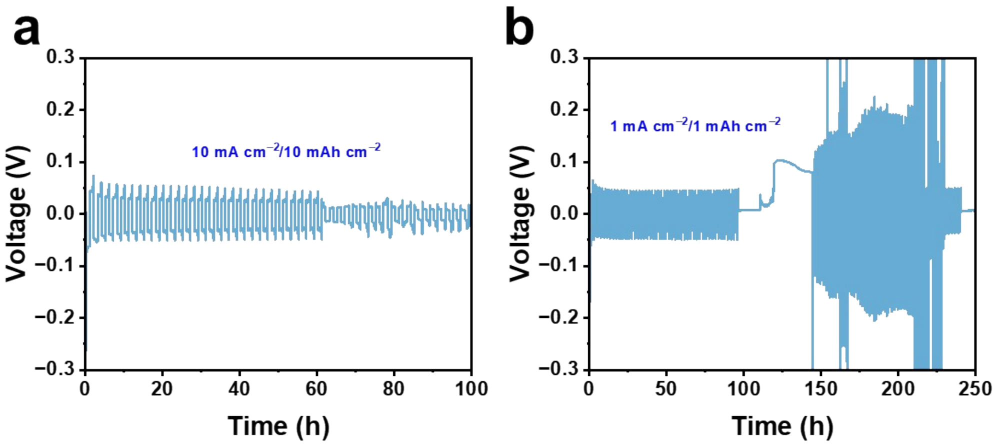

Fig. S12. Cycling performance of Zn||Zn cells using liquid electrolyte (a) under large current density and capacity of 10 mA cm^{-2}/10 mAh cm^{-2} and (b) alternating test between Zn plating−stripping with working (48 h) and resting (48 h).

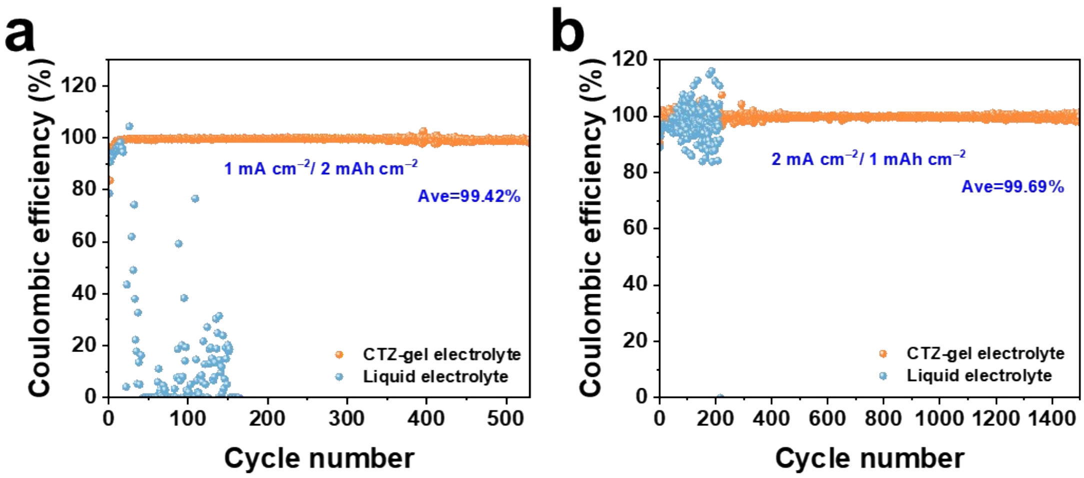

Fig. S13. Coulombic efficiency profiles of Zn||Cu cells with the two electrolytes at (a) 1 mA cm^{-2}/2 mAh cm^{-2} and (b) 2 mA cm^{-2}/1 mAh cm^{-2}.

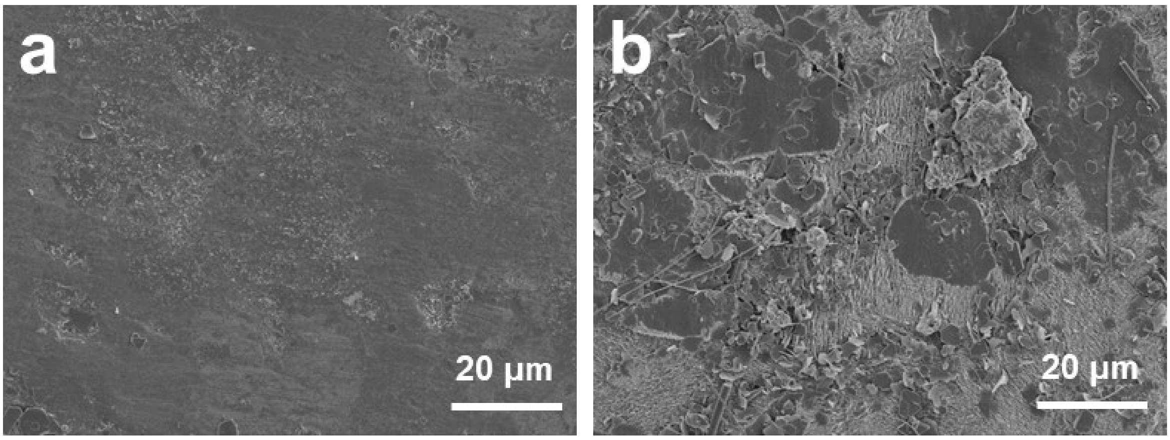

Fig. S14. Surface FE-SEM images of Zn foils at deposited state after cycling (1 mA cm^{-2}/1 mAh cm^{-2}) after 50 cycles in the Zn||Zn symmetrical cells with the (a) CTZ-gel and (b) liquid electrolyte.

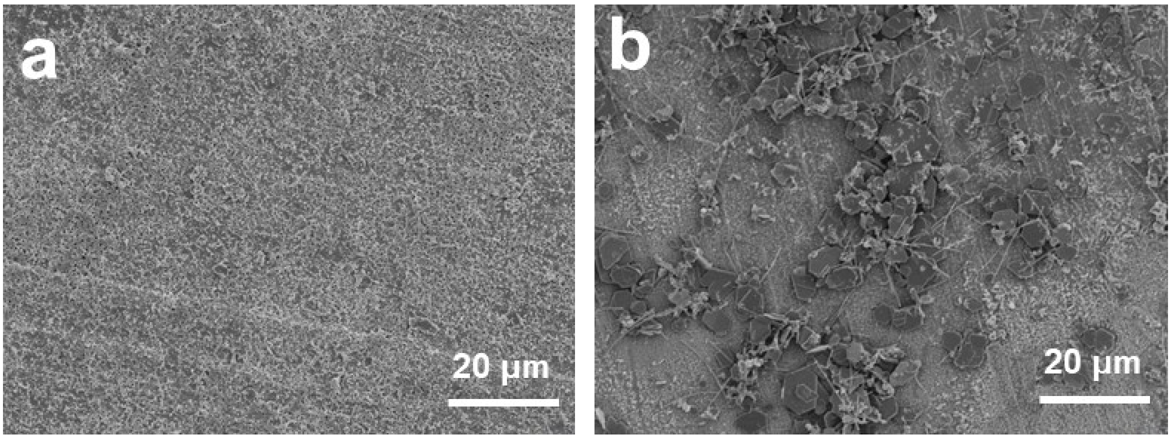

Fig. S15. Surface FE-SEM images of Cu foils at deposited state after cycling (1 mA cm^{-2}/1 mAh cm^{-2}) after 50 cycles in the Zn||Cu asymmetrical cells with the (a) CTZ-gel and (b) liquid electrolyte.

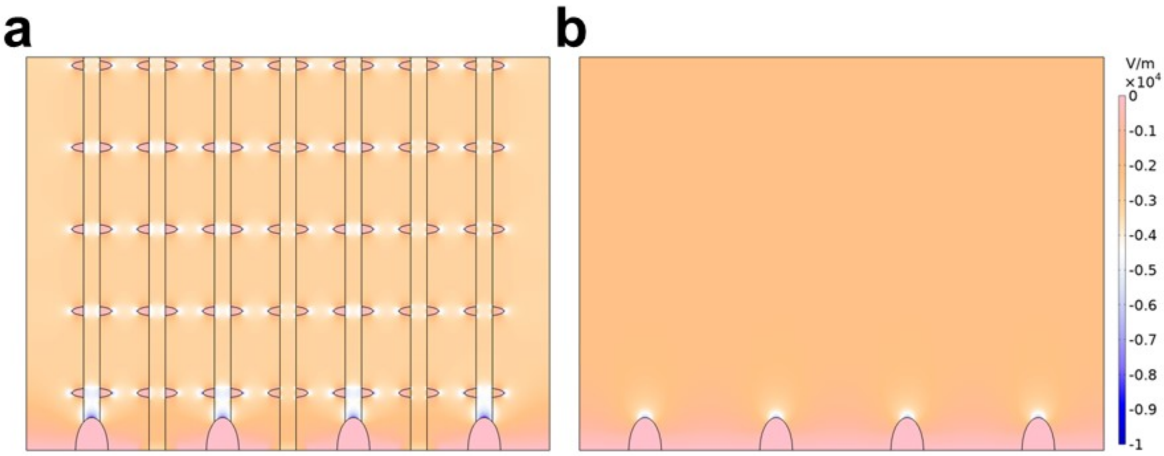

Fig. S16. COMSOL simulations for the electrical field on Zn electrode with the (a) CTZ-gel and (b) liquid electrolyte during plating.

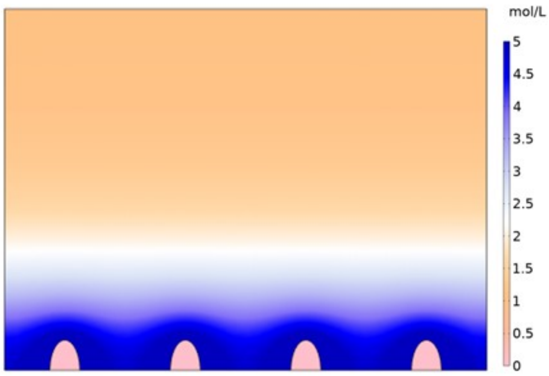

Fig. S17. COMSOL simulations for the Zn^{2+} flux on the Zn electrode with liquid electrolyte during plating.

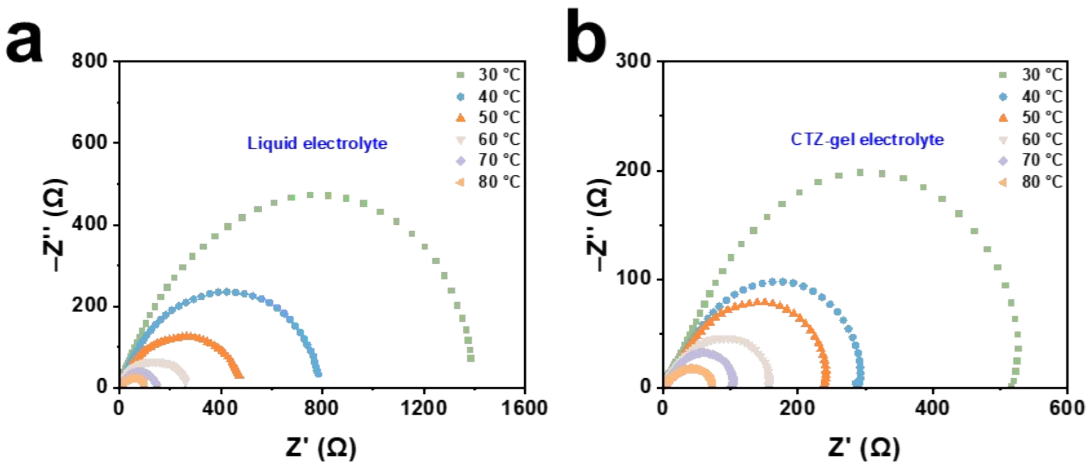

Fig. S18. Nyquist plots of the pristine Zn||Zn cells with (a) the liquid and (b) CTZ-gel electrolytes at different temperatures for the calculations of desolvation activation energies.

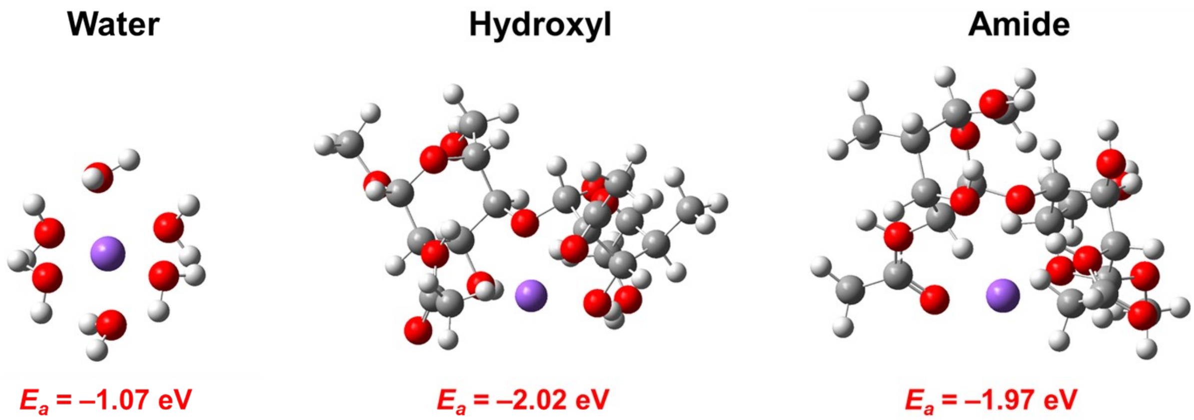

Fig. S19. Simplified models for DFT calculations of binding energies of Zn^{2+} ion in different electrolytes.

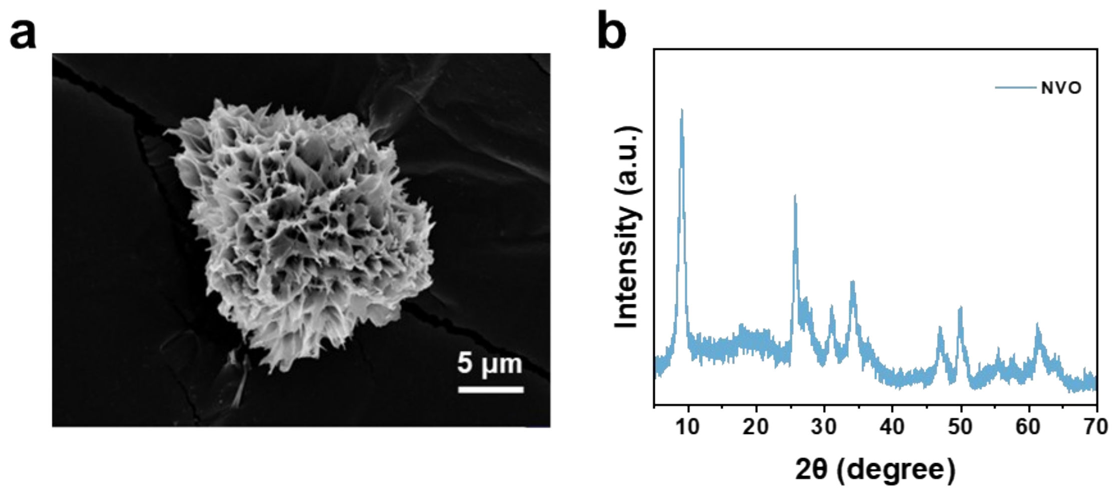

Fig. S20. (a) FE-SEM image and (b) XRD pattern of the NVO powder.

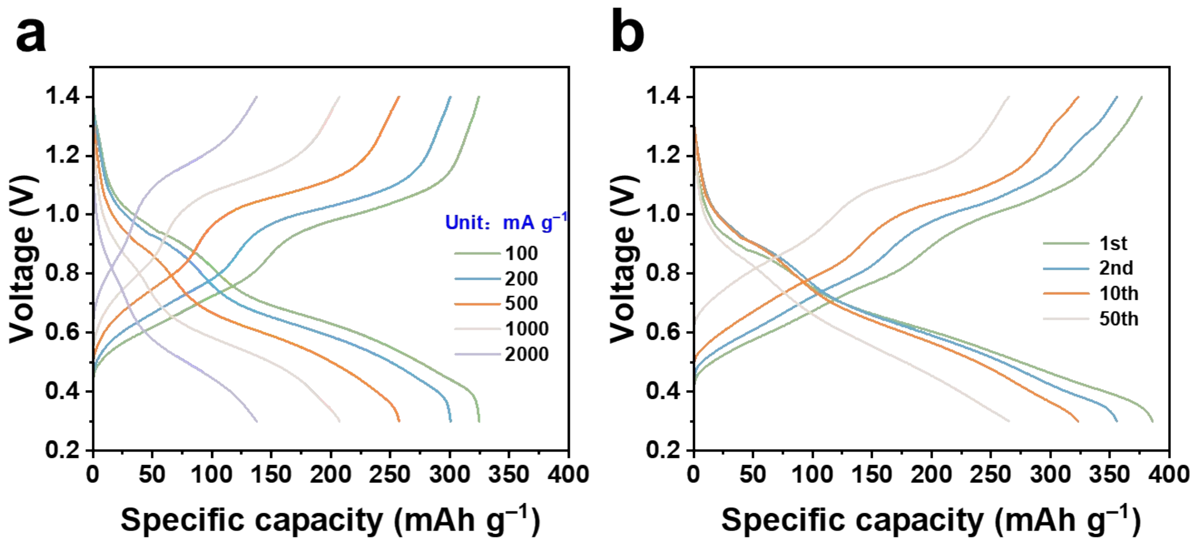

Fig. S21. Charge–discharge curves of Zn||NVO cells using liquid electrolyte (a) under different current rates from 100 to 2000 mA g^{-1} and (b) cycling at 500 mA g^{-1} with different cycle numbers.

Table S1. The mechanical properties comparison between the CTZ-gel electrolyte and other reported natural polymer-based electrolyte for AZBs.

Hydrogel electrolyte	Electrolyte salt	Toughness ($MJ\ m^{-3}$)	Elastic modulus (MPa)	Biodegradability	Ref.
CTZ-gel	**2 M $ZnSO_4$**	**0.65**	**6.82**	**Yes**	**This work**
DCZ-gel	2 M $Zn(OTf)_2$	1.20	1.93	Yes	2
TCh	2 M $ZnSO_4$	156	2600	Yes	3
ZA	2 M $ZnSO_4$	3.78	4.63	Yes	4
SCS	2 M $ZnSO_4$	0.09	0.04	No	5
PAM/CMC/XG	1 M $Zn(CF_3SO_3)_2$	0.24	0.02	No	6
GAME	2 M $ZnSO_4$	1.5	3.00	Yes	7
Ani-gel	3 M $Zn(ClO_4)_2$	0.032	0.01	Yes	8
PACB	2 M $ZnSO_4$	0.19	0.08	No	9
CNF-PAM	2 M $Zn(CF_3SO_3)_2$	0.81	0.05	No	10
BBAS	3 M $Zn(ClO_4)_2$	0.04	0.01	No	11
CD-PEO/PAM	1 M $Zn(OTf)_2$	0.85	0.04	No	12
Gel-PUZ	2 M $ZnSO_4$	0.02	0.10	No	13
Gel/SA-acetate	2 M $ZnSO_4$	0.75	0.65	No	14
HE-PAM	2 M $ZnSO_4$	0.15	0.25	No	15

Table S2. The electrochemical performance comparison between the CTZ-gel electrolyte and other reported natural polymer-based electrolyte for AZBs.

Hydrogel electrolyte	Zn‖Zn cell			Zn‖Cu cell		Full cell			Ref.
	Current density/capacity ($mA\ cm^{-2}$/$mAh\ cm^{-2}$)	Cycle life (h)	Maximum Cumulative capacity (Ah)	Current density ($mA\ cm^{-2}$)	Average CE (%)/ cycles	Cathode material	Reversible capacity ($mAh\ g^{-1}$)/ Current density ($A\ g^{-1}$)	Capacity retention (%)/ Number of cycles	
CTZ-gel	**1/1** **10/10**	**2500** **420**	**2.10**	**1** **2**	**99.6/2000** **99.7/1500**	**$NH_4V_4O_{10}$**	**334/0.5** **202/2**	**86/200** **80/1500**	**This work**
DCZ-gel	0.5/0.5	2000	0.50	5	99.4/2000	PANI/CC	160/0.5	85/200	2
TCh	10/10	320	1.60	5	98.9/600	MnO_2	190/1.5	93/800	3
ZA	2/0.25	2000	2.00	1	99.4/1000	MnO_2	214/2	—/500	4
SCS	1/1	2500	1.25	1	99.4/1200	$NH_4V_4O_{10}$	233/1	96/500	5
PAM/CMC/X	1/1	230	0.12	2	99.3/380	GCNF	93/10	84/10000	6
GAME	0.5/0.5	400	0.10	1	99/300	V_2O_5/CNT	212/2	85/200	7
Ani-gel	2/2	1200	1.20	1	98/300	MnO_2	56/1	75/1000	8
PACB	1/1	2100	1.05	10	99.2/1000	$NH_4V_4O_{10}$	180/0.5	71/1000	9
CNF-PAM	1/1	500	0.25	—	—	MgVO	214/10	—/4000	10
BBAS	10/10	300	1.5	5	98/2000	I_2	147/2	—/1000	11
CD-PEO/PAM	1/1	180	0.09	—	—	V_2O_5	180/5	90/3500	12
Gel-PUZ	0.1/0.1	2300	0.12	1	98.0/700	I_2	110/0.5	85/1500	13
Gel/SA-acetate	0.1/0.1	1600	0.08	1	99.9/5600	activated	110/20	99/15000	14
HE-PAM	0.1/0.1	1500	0.08	—	—	MnO_2	125/10	80/2000	15

Table S3. R_{ct} values of Zn||Zn cells with the liquid and CTZ-gel electrolyte obtained from Figure S15.

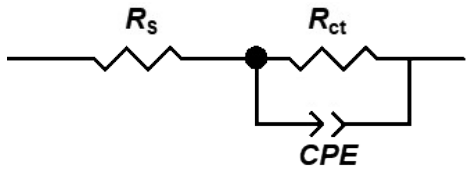

Temperature (°C)	Liquid electrolyte (Ω)	CTZ-gel electrolyte(Ω)
30	1473	626
40	812	328
50	484	273
60	263	173
70	148	112
80	99	76

References

1. B. Tang, J. Zhou, G. Fang, F. Liu, C. Zhu, C. Wang, A. Pan and S. Liang, *J. Mater. Chem. A*, 2019, **7**, 940-945.

2. H. Zhang, X. Gan, Y. Yan and J. Zhou, *Nano-Micro Lett.*, 2024, **16**, 106.

3. Q. Wang, J. Zhao, J. Zhang, M. Li, F. Tan, X. Xue, Z. Sui, Y. Zou, X. Zhang, W. Zhang and C. Lu, *Adv. Funct. Mater.*, 2024, **34**, 2405957.

4. L. Hong, X. Wu, Y.-S. Liu, C. Yu, Y. Liu, K. Sun, C. Shen, W. Huang, Y. Zhou, J.-S. Chen and K.-X. Wang, *Adv. Funct. Mater.*, 2023, **33**, 2300952.

5. Y. Hu, Z. Wang, Y. Li, P. Liu, X. Liu, G. Liang, D. Zhang, X. Fan, Z. Lu and W. Wang, *Chem. Eng. J.*, 2024, **479**, 147762.

6. J. Gao, F. Guo, C. Ji, X. He, H. Mi and J. Qiu, *J. Mater. Chem. A*, 2022, **10**, 24639-24648.

7. Y. Lu, T. Zhu, N. Xu and K. Huang, *ACS Appl. Energy Mater.*, 2019, **2**, 6904-6910.

8. Y. Zhang, M. Chen, J. Lu, H. Ma, W. Liu, J. Yu, Q. Tian, J. Xu and J. Chen, *Chem. Eng. J.*, 2025, **506**, 159950.

9. G. Liu, S. Zhang, Y. Peng, M. Yu, L. Zhao, J. Zhang, Y. Meng and F. Ran, *J. Colloid Interface Sci.*, 2025, **678**, 159-167.

10. W. Xu, C. Liu, S. Ren, D. Lee, J. Gwon, J. C. Flake, T. Lei, N. Baisakh and Q. Wu, *J. Mater. Chem. A*, 2021, **9**, 25651-25662.

11. Y. Liu, F. Li, J. Hao, H. Li, S. Zhang, J. Mao, T. Zhou, R. Wang, L. Zhang and C. Zhang, *Adv. Funct. Mater.*, 2024, **34**, 2400517.

12. H. Xia, G. Xu, X. Cao, C. Miao, H. Zhang, P. Chen, Y. Zhou, W. Zhang and Z. Sun, *Adv. Mater.*, 2023, **35**, 2301996.

13. X. Zhou, S. Huang, L. Gao, Z. Zhang, Q. Wang, Z. Hu, X. Lin, Y. Li, Z. Lin, Y. Zhang, Y. Tang, Z. Wen, M. Ye, X. Liu and C. C. Li, *Angew. Chem. Int. Ed.*, 2024, **63**, e202410434.

14. C. Tian, J. Wang, R. Sun, T. Ali, H. Wang, B.-B. Xie, Y. Zhong and Y. Hu, *Angew. Chem. Int. Ed.*, 2023, **62**, e202310970.

15. Z. Shen, Y. Liu, Z. Li, Z. Tang, J. Pu, L. Luo, Y. Ji, J. Xie, Z. Shu, Y. Yao, N. Zhang and G. Hong, *Adv. Funct. Mater.*, 2025, **35**, 2406620.